Binding and Relaxometric Properties of Heme Complexes with Cyanogen Bromide Fragments of Human Serum Albumin

Enrico Monzani,* Maria Curto,* Monica Galliano,† Lorenzo Minchiotti,† Silvio Aime,‡ Simona Baroni,‡ Mauro Fasano,§ Angela Amoresano,¶ Anna Maria Salzano,¶ Piero Pucci,¶ and Luigi Casella*

*Dipartimento di Chimica Generale and †Dipartimento di Biochimica, Università di Pavia, 27100 Pavia, Italy; ‡Dipartimento di Chimica, Università di Torino, 10125 Torino, Italy; §Dipartimento di Biologia Strutturale e Funzionale, Università dell'Insubria, 21100 Varese, Italy; and ¶Dipartimento di Chimica Organica e Biochimica, Complesso Universitario Monte S'Angelo, Università di Napoli Federico II, 80126 Napoli, Italy

ABSTRACT The spectroscopic and reactivity properties of hemin complexes formed with cyanogen bromide fragments B (residues 1–123), C (124–298), A (299–585), and D (1–298) of human serum albumin (HSA) have been investigated. The complex hemin-D exhibits binding, spectral, circular dichroism, and reactivity characteristics very similar to those of hemin-HSA, indicating that fragment D contains the entire HSA domain involved in heme binding. The characteristics of the other hemin complexes are different, and a detailed investigation of the properties of hemin-C has been carried out because this fragment contains the HSA binding region of several important drugs. Hemin-C contains a low-spin Fe(III) center, with two imidazole ligands, but the complex undergoes a reversible structural transition at basic pH leading to a high-spin, five-coordinated Fe(III) species. This change determines a marked increase in the relaxation rate of water protons. Limited proteolysis experiments and mass spectral analysis carried out on fragment C and hemin-C show that the region encompassing residues Glu-208 to Trp-214 is protected from activity of proteases in the complex and, therefore, is involved in the interaction with hemin. A structural model of fragment C enables us to propose that His-242 and His-288 are the axial ligands for the Fe(III) center.

INTRODUCTION

Heme is one of the most versatile prosthetic groups present in metalloproteins, which play important roles in electron transfer reactions, oxygen transport and storage, and a variety of oxidation processes that use dioxygen, hydrogen peroxide, or alkyl peroxides as terminal oxidants (Kadish et al., 1999; Xie and Dolphin, 1994; Dawson, 1988). In addition, heme serves regulatory functions in many biological processes such as protein synthesis (Ochoa and de Haro, 1979), cellular growth and differentiation (Sassa, 1988), and the activation of soluble guanylate cyclase by nitric oxide (Ignarro et al., 1982). Heme is released in plasma upon rupture of red blood cells in many events, including hemolysis, trauma and ischemia reperfusion (Jacob, 1994). In these conditions, it is currently thought that human serum albumin (HSA) and hemopexin serve as traps for extracellular heme, to prevent its toxic effects and convey it to its specific catabolism site (Balla et al., 1993). However, Miller and Shaklai (1999) have recently reported that HSA and hemopexin are not capable of preventing oxidative damage of low-density lipoprotein by the transient hemin. Hemopexin is the strongest heme-binding protein in plasma (K_b 10^9 M^{-1} (Hrkal et al., 1974)), and in normal conditions albumin rapidly transfers the heme to hemopexin. However, the abundance of hemopexin in plasma is low (10–20 μM), and albumin can thus play an important role as heme carrier in conditions where hemopexin is saturated (Peters, 1996). Some recent results from reactivity studies may extend the currently accepted role and significance of heme binding by HSA. In fact, we have found that the hemin-HSA complex exhibits catalase and peroxidase activity (Monzani et al., 2001). Although this activity is weak, considering the large abundance of HSA, it may contribute to the antioxidant defense in the extracellular fluids of the human body, where the presence of antioxidant enzymes is scarce.

Although a detailed structural description of the heme binding site in HSA is lacking, insight into its position has been obtained by circular dichroism (CD) studies of the complexes between ferric heme and the three recombinant HSA domains I (residues 1–197), II (residues 189–385), and III (residues 381–585) (Dockal et al., 1999). Based on these studies, it was concluded that the main contribution to the HSA primary binding site for hemin is due to domain I. Other studies aimed at addressing the location of the heme binding site were performed using the large cyanogen bromide fragments of HSA (Hrkal et al., 1978), and in this case, it was proposed that the heme binding site is mainly included in the HSA middle region corresponding to fragment C (residues 124–298) (Hrkal et al., 1978). Spectroscopic studies on various derivatives of the hemin-HSA complex (Casella et al., 1993; Monzani et al., 2001; Fasano et al., 2001) and docking simulations (Fasano et al., 2001) based on the crystal structure of HSA (He and Carter, 1992) suggest that the heme iron center is axially bound to a histidine and possibly to a tyrosine residue. This type of detailed analysis is currently unavailable for the hemin complexes formed by the HSA fragments. In the present

Submitted March 5, 2002, and accepted for publication June 7, 2002.

Address reprint requests to Dr. Luigi Casella, Dipartimento di Chimica Generale, Via Taramelli 12, 27100 Pavia, Italy. Tel.: 39-0382-507331; Fax: 39-0382-528544; E-mail: bioinorg@unipv.it.

0006-3495/02/10/2248/11 $2.00

paper we report the binding and spectral properties as well as the reactivity of the hemin complexes of the cyanogen bromide fragments of HSA, which, according to Lapresle (Doyen et al., 1982), here will be designated as B (residues 1–123), C (residues 124–298), and A (residues 299–585). An additional fragment, D (residues 1–298), made of B and C, which is a result of the incomplete cleavage of the peptide bond between Met-123 and Cys-124 was also used (Doyen et al., 1982). For the adduct of fragment C with hemin (hemin-C) and its analog with Mn(III)-protoporphyrin IX (Mn(III)-PPIX-C), containing Mn(III) in the place of Fe(III), the relaxometric properties were investigated. Moreover, the interaction between hemin and fragment C has been studied by limited proteolysis and mass spectrometry. The combination of the various approaches allowed us to obtain a structural description of the heme environment in this albumin fragment and showed that, although it is not fully representative of the heme binding site, it contains a portion of the HSA high-affinity site for the ligand.

MATERIALS AND METHODS

Materials

HSA was purified from fresh serum by anion-exchange chromatography on a DEAE Sephadex, column and the purity of the protein was checked by SDS-PAGE (Galliano et al., 1990). The HSA fragments were prepared according to Lapresle and Doyen (1975) with slight modifications. The unreduced protein was treated with cyanogen bromide in 70% formic acid, and the four fragments were fractionated by gel filtration on a Superdex 75 column (80 × 1.6 cm) equilibrated with 5% propionic acid and 0.15 M NaCl followed by ion-exchange chromatography on carboxymethyl (CM) cellulose (2.5 × 10 cm) equilibrated with 0.01 M phosphate buffer, pH 2.7, and eluted with a linear gradient from 0.05 to 0.3 M NaCl. The molar extinction coefficients of the fragments were calculated on the basis of their amino acid sequence with the Compute tool of ExPASy (http://www.expasy.ch) at the University of Geneva, Switzerland. Hemin chloride, trypsin treated with L-tosylamido-2-phenylethyl chloromethyl ketone, chymotrypsin, subtilisin, and protease V8 were purchased from Sigma Chemical Co. (St. Louis, MO). All other chemicals (from Sigma) were reagent grade and used as received. Aqueous buffers were prepared from double-distilled water. Hydrogen peroxide solutions for kinetic experiments were prepared by dilution of a 30% aqueous solution and were standardized by iodimetry. UV-Vis and CD spectra were measured with HP8452A (Hewlett-Packard, Waldbronn, Germany) and CADAS (Dr. Lange, Berlin, Germany) spectrophotometers and a J710 (Jasco Europe, Cremella, Italy) dichrograph, respectively. The RP-HPLC C18 column (250 × 2.1 mm) was purchased from Phenomenex (Palo Alto, CA).

Binding experiments

Binding experiments of hemin or Mn(III)-PPIX to the HSA fragments were studied spectrophotometrically using an optical cell with 10-cm path length. A small amount of a solution of hemin in dimethylsulfoxide (DMSO; $\sim 3\times10^{-3}$ M) was diluted in the optical cell in a solvent mixture of DMSO-aqueous 0.1 M phosphate buffer, pH 7.0, 1:10 (v/v), or 2:10 (v/v) in the case of fragment D (final protein concentration $\sim 5 \times 10^{-7}$ M). This solution was titrated with the HSA fragment by adding small amounts of an ~0.3 mM protein solution in the aqueous buffer and recording the spectrum after incubation for a few minutes after each addition. Difference spectra with respect to hemin were taken, and the binding isotherm was analyzed by plotting the difference of absorbance between the maximum and the minimum of the two-signed difference spectra against the protein concentration. The equation derived for a high-affinity equilibrium was applied to fit the binding data (Monzani et al., 2001).

Kinetics

The kinetic experiments on the catalytic oxidation of phenolic substrates by hydrogen peroxide in the presence of hemin-HSA fragments were carried out in a magnetically stirred and thermostated optical cell of 1-cm path length, at 25.0 ± 0.1°C, in 0.1 M phosphate buffer, pH 7.0, following procedures described previously for the reactions catalyzed by the hemin-HSA complex (Monzani et al., 2001). The phenolic substrates studied were *p*-cresol, *p*-hydroxyphenyl propionic acid, tyramine, and L- and D-tyrosine. For each substrate, the reaction rates were studied as a function of both hydrogen peroxide and substrate concentrations. The reactions were followed spectrophotometrically at 300 nm, where the dimeric products of phenol coupling absorb (Casella et al., 1994). The initial rates were determined from the linear part of the plots of Δabsorbance versus time. The $\Delta\epsilon$ values necessary to convert the rate data from Δabsorbance/s to M/s were reported previously (Monzani et al., 2001).

NMR relaxation

Water proton T_1 measurements were obtained on a Stelar SpinMaster Spectrometer (Stelar, Mede, Italy) operating at 20 MHz, by means of the inversion-recovery technique (16 experiments; 4 scans) (Braun et al., 1998). Magnetization values were obtained by averaging the first 128 data points of the free induction decay. A typical 90° pulse width was 3.5 μs. The reproducibility in T_1 measurements was ±0.5%. The temperature was controlled by a Stelar VTC-91 airflow heater, equipped with a copper-constantan thermocouple; the actual temperature in the probe head was measured with a Fluke 52 k/j digital thermometer (Fluke, Zürich, Switzerland), with an uncertainty of ±0.3°C.

Values of r_{1p} were determined by subtracting from the observed relaxation rate (R_1^{obs}) the blank relaxation rate value (R_1^{dia}) measured for solutions containing the HSA fragment in the same concentration without the paramagnetic prosthetic group.

Variable temperature ^{17}O-NMR linewidth measurements were recorded at 9.4 T on a JEOL EX-400 spectrometer (JEOL, Tokyo, Japan), equipped with a 5-mm inner diameter probe head, with a D_2O external lock. Sample solutions were supplemented with enriched $H_2{}^{17}O$ (Cortec, Paris, France) to an isotopic abundance of 2.6%. Experimental settings were 22-kHz spectral width, 90° pulse for 14 μs, 0.75-s acquisition time, 256 scans, and no sample spinning.

Limited proteolysis experiments

Limited proteolysis experiments were carried out by incubating fragment C or the hemin-C complex with trypsin, chymotrypsin, subtilisin, and protease V8 as enzymatic probes. Digestions were all performed in 100 mM sodium phosphate (pH 7.0) containing 8% DMSO, at 30°C and using various enzyme to substrate (E/S) ratios (w/w). The extent of the reaction was monitored on a time course basis by sampling the incubation mixture at different time intervals. Digested protein samples were acidified by adding trifluoroacetic acid (TFA) to lower the pH. Peptide mixtures from the different proteolysis experiments were fractionated by reverse-phase HPLC on a Phenomenex C18 column. Peptides were eluted by means of a linear gradient from 5% to 60% of acetonitrile in 0.1% aqueous TFA over 60 min, and elution was monitored at 220 and 280 nm. Fractions were manually collected and identified by electrospray mass spectrometry ES/MS.

The complex hemin-C was formed by incubation of fragment C in 100 mM sodium phosphate, pH 7.0, and a 10-fold molar excess of a hemin solution in DMSO to obtain 8% DMSO as a final concentration; the complex was then allowed to form for 10 min at 30°C before the protease addition.

Mass spectrometry

Protein samples and proteolytic fragments were analyzed by ES/MS using an API 100 single-quadrupole mass spectrometer (Applied Biosystems, Firmingham, MT) equipped with an ion spray source. Samples were injected into the atmospheric pressure ion source via a syringe pump at a flow rate of 5 μl/min. Data were acquired and elaborated with the software provided by the manufacturer. Mass calibration was performed by means of multiply charged ions from a separate injection of horse heart myoglobin (Sigma; average molecular mass, 16,951.5 Da); all masses are reported as average values.

ES/MS analysis of fragment C and hemin-C

Fragment C was eluted from a Phenomenex C4 column by means of a linear gradient from 20% to 65% of acetonitrile in 0.1% aqueous TFA over 30 min; elution was monitored at 220 and 280 nm. The molecular weight of the HPLC-purified peptide was determined by ES/MS analysis.

The hemin-C complex was formed in 100 mM phosphate buffer, 1% cetyltrimethylammonium bromide (cTAB), pH 7, and then subjected to gel filtration chromatography on a PD10 prepacked column (Sephadex G25, Pharmacia, Uppsala, Sweden), eluted with 50 mM ammonium acetate, pH 7.0. The complex (10 pmol/μl) was directly injected into the ion source of the API 100 mass spectrometer. Instrumental parameters for the mass analysis were appropriately set to avoid complex dissociation in the gaseous phase.

Structural analysis

Structural analysis, including electrostatic potential surface calculations, was performed by means of the Swiss-PdbViewer version 3.7 b2 (Guex and Peitsch, 1997).

RESULTS

Spectra and binding characteristics

The electronic spectrum of hemin in a dilute solution of 10% DMSO-aqueous phosphate buffer at pH 7.0 exhibits the typical features of high-spin ferric heme (Owens and O'Connor, 1988): Soret band at 400 nm, β band at 498 nm, α band almost absent, and charge transfer (CT) band at 620 nm. In the spectrum of the hemin-HSA adduct recorded in the same conditions, the Soret band broadens and shifts to 404 nm, and new contributions to the spectrum are given by a detectable α band at 530 nm and a CT band at 580 nm (Monzani et al., 2001). The spectral features of the hemin-D complex are similar to those of hemin-HSA but with a larger contribution by the low-spin component, as shown by the more prominent α band at 532 nm (Fig. 1 *A*). By contrast, the spectrum of the hemin-C complex appears to be totally low spin: sharp Soret band at 412 nm and β and α bands at 534 and 566 nm, respectively. The spectrum of this complex exhibits a pronounced pH dependence, with a reversible shift of the Soret band to 394 nm in basic solution (pH $>$ 10).

Hemin binds to fragment A essentially as a low-spin species, as suggested by the Soret band at 414 nm and β and α bands at 534 and 566 nm, respectively, but the presence of a small fraction of high-spin species is indicated by the CT shoulder near 630 nm (Fig. 1 *A*). Finally, the electronic spectrum of hemin-B resembles that of free hemin, although even in this case a slight broadening of the Soret band at lower energy and a detectable shoulder near 530 nm, corresponding to an α band indicate the existence of a small fraction of low-spin form. Note that the spectra of hemin-A and especially hemin-B obtained in our conditions are much sharper in the Soret region than those reported previously by Hrkal et al. (1978), probably because these authors studied the complexes between hemin and HSA fragments in aqueous buffer (without addition of DMSO), where hemin is aggregated. Because HSA itself is hardly able to destroy the aggregates and bind monomeric hemin (Kuzelova et al., 1997), it is likely that the same problem occurs with HSA fragments.

Complementary information could be obtained by replacing ferric heme with the analog Mn(III)-PPIX complex, as already reported for hemin-HSA (Fasano et al., 2001). At pH 7.0 (phosphate buffer 0.1 M), Mn(III)-PPIX-C exhibits a strong absorption at 369 nm, with minor bands at 468 and 559 nm. This pattern resembles that observed for Mn(III)-PPIX-HSA (i.e., 370, 465, and 561 nm for γ, β, and α bands, respectively) and supports the evidence for a six-coordinated heme complex for Mn(III) as well. Although the γ band is almost unaffected by the pH value, the β band appears to be more diagnostic; actually, a shift from 467 to 447 nm is observed for Mn(III)-PPIX-HSA on going from pH 6 to 10. The same behavior is shown by the α band, which is red-shifted from 556 to 571 nm. According to the proposed mechanism, the spectral changes are the result of the displacement of a water molecule by a tyrosyl oxygen as the sixth ligand of Mn(III)-PPIX (Fasano et al., 2001). In the case of Mn(III)-PPIX-C, β and α bands undergo only modest shifts from 468 to 464 nm and from 559 to 563 nm, respectively. These figures cannot be associated with a change of the coordination state of the metal ion, as it occurs with hemin-C, or ligand exchange, as it occurs with Mn(III)-PPIX-HSA, as a function of pH. It is likely that Mn(III) is bound to two axial histidines in Mn(III)-PPIX-C, as is Fe(III) in hemin-C, but that neither of the histidine ligands is released in basic medium, because of the stronger preference of Mn(III)-porphyrins for imidazole ligands with respect to the Fe(III) analogs (Mashiko and Dolphin, 1987). Spectral features similar to Mn(III)-PPIX-C and Mn(III)-PPIX-HSA are observed for Mn(III)-PPIX-D: γ, β, and α bands occur at 369, 465, and 556 nm (pH 7.0), with an appreciable shift in basic medium, i.e., at 364, 465, and 567 nm (pH 10.5), respectively. In this case it is difficult to draw any firm con-

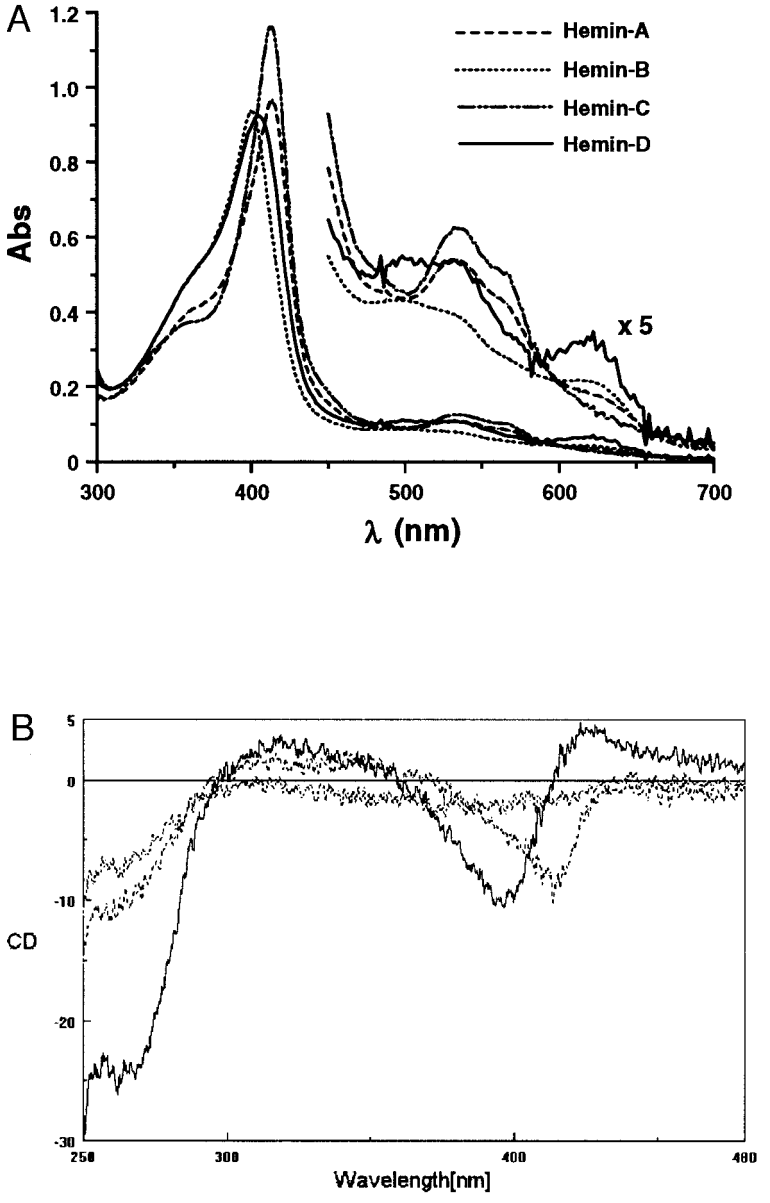

FIGURE 1 (*A*) Electronic spectra of hemin complexes with HSA fragments A (— — —), B (· · ·), C (— · · —), and D (——) in DMSO-aqueous 0.1 M phosphate buffer, pH 7.0, 1:10 (v/v), or 2:10 (v/v) in the case of fragment D. Concentrations of the adducts were $\sim 5 \times 10^{-7}$ M, and path length was 10 cm. (*B*) Circular dichroism spectra of hemin complexes with HSA fragment B (*gray trace*), C (*dotted trace*), and D (*black trace*) (same conditions as above).

clusion about the manganese axial ligands, although the spectral behavior resembles more that of Mn(III)-PPIX-C than that of Mn(III)-PPIX-HSA.

By titrating solutions of hemin in a DMSO-aqueous buffer at pH 7.0 with the HSA fragments it has been possible to estimate the affinity of hemin for the various polypeptides. The use of DMSO in these experiments is convenient to prevent heme aggregation in aqueous solution. The plots obtained from difference spectra were in fact well behaved, and the resulting binding constants are collected in Table 1. DMSO affects the value of the binding constants only marginally. For instance, the K_b value of hemin for HSA that we found in DMSO-aqueous buffer 10% (v/v), $(3.4 \pm 0.6) \times 10^7$ M^{-1} (Monzani et al., 2001), is only slightly lower than that determined in pure buffer through fluorescence measurements, 5×10^7 M^{-1} (Beaven et al., 1974). We have also found here that on increasing the amount of DMSO in the solution from 10% to 20% (v/v) the

TABLE 1 Binding constants of hemin and Mn(III)-PPIX to HSA fragments in DMSO-aqueous 0.1 M phosphate buffer, pH 7.0, at 20°C

Complex	K_b (M^{-1})
Hemin-A	$(2.1 \pm 0.1) \times 10^6$
Hemin-B	$(1.3 \pm 0.1) \times 10^5$
Hemin-C	$(9.3 \pm 0.3) \times 10^5$
Hemin-D	$(2.6 \pm 0.3) \times 10^7$
Mn(III)-PPIX-C	$(6.1 \pm 3.4) \times 10^6$
Mn(III)-PPIX-D	$(3.1 \pm 1.7) \times 10^6$

K_b value of hemin for fragment C slightly decreases to $(5.5 \pm 0.3) \times 10^5\ M^{-1}$. The K_b value reported for hemin-D in Table 1 is only slightly lower than that determined for hemin-HSA (Monzani et al., 2001). For the other fragments the affinity of hemin is significantly lower than for the intact protein, but we note that the values of the binding constants that we find here are significantly larger than those reported previously by Hrkal et al. (1978), particularly for hemin-A and hemin-B. Likely, this is because of the same problem of heme aggregation in aqueous buffer solution discussed above. The affinity of Mn(III)-PPIX for HSA fragments C and D has been measured as well. Unlike hemin, this complex shows comparable affinities for the two polypeptides, with a slightly larger value of the binding constant in the case of fragment C (Table 1).

The affinity of Mn(III)-PPIX for these fragments is comparable with that for HSA.

Circular dichroism spectra.

The far-UV CD spectra of HSA fragments A, B, and C were reported previously by Hrkal et al. (1978). The spectra indicated significant portions of α-helical structure, comparable with that of HSA. In the CD spectrum of fragment D, the α-helical content is further slightly increased (data not shown). We also investigated the effect of hemin binding to the four HSA fragments in the CD spectra. It was found that the binding occurs without any significant change in the far-UV CD features of the peptides, but changes are observable in some cases in the near-UV region, where the HSA fragments exhibit a broad negative band near 260 nm, which is only partially resolved from the more intense negative CD activity at higher energy. The intensity of this aromatic CD band increases in the order of B < C < A < D. However, upon binding of hemin to the HSA fragments, the CD activity of the aromatic envelope remains basically unaffected for A and B, whereas it is slightly strengthened for C and strongly enhanced in the case of D. For hemin-C and hemin-D, additional CD activity of positive sign occurs in the range between 300 and 350 nm. The increase of optical activity in the aromatic region for these complexes parallels the behavior observed for hemin binding to HSA (Monzani et al., 2001) and can be attributed to reduced conformational mobility of the aromatic residues of the proteins in the binding site.

The CD spectra of the hemin complexes with the four HSA fragments are particularly informative in the visible region, where the induced CD activity in the porphyrin chromophore is observed. These spectra show remarkable differences (Fig. 1 *B*). Hemin-D exhibits a major negative peak near 395 nm and a minor positive peak near 420 nm. For hemin-C the spectrum is different and features a single negative peak near 415 nm, practically coincident with the Soret absorption maximum. For hemin-A the CD activity is extremely weak, and for hemin-B the CD is basically absent.

The CD spectrum of hemin-C undergoes reversible changes with pH that parallel the changes observed in the electronic spectrum. On increasing the pH from 7.0 to 10.0 a progressive decrease in the negative CD peak at 415 nm and an increase of the broad CD activity of positive sign between 350 and 400 nm, featuring a maximum near 385 nm, occur. Isodichroic points are observable near 280 and 340 nm. Overall, the optical activity within the Soret band is reduced by more than 50% in the basic pH range, and the protein CD band near 260 nm becomes weaker and less defined.

Kinetics

For comparative purposes, we chose to investigate the peroxidase-like activity of the present hemin complexes with the same group of phenolic substrates previously studied with hemin-HSA (Monzani et al., 2001), namely, *p*-cresol (1), *p*-hydroxyphenyl propionic acid (2), tyramine (3), and L- and D-tyrosine (L-4 and D-4). Given the similarity in general behavior with hemin-HSA, the same catalytic mechanism can be assumed for the hemin complexes with HSA fragments. This is reproduced in Scheme 1, where E is the hemin-peptide complex, E_A the active species, S the substrate, E_S the hemin-peptide-substrate ternary complex, E_{AS} the corresponding active species-substrate complex, k_1 the active species formation constant, k'_1 the kinetic constant for the transformation of E_S into E_{AS}, k_P the kinetic constant for product formation, k_C and k'_C the kinetic constants for decomposition of peroxide by E_A and E_{AS}, respectively, and K_B and K'_b the substrate affinity constants for E and E_A, respectively (Monzani et al., 2001).

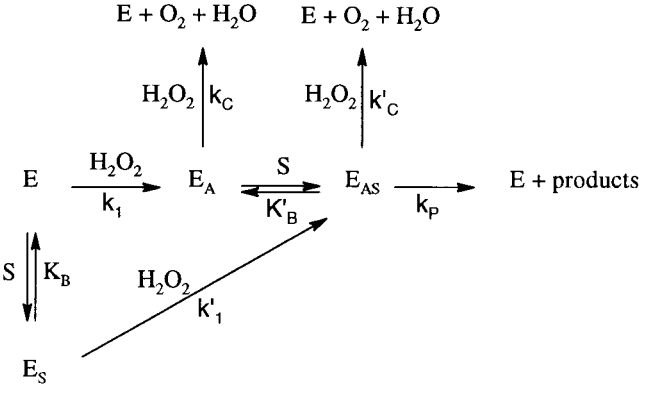

Scheme 1.

Under the assumptions described for hemin-HSA catalysis (Monzani et al., 2001) and operating under saturating

TABLE 2 Kinetic constants k_1' (M^{-1} s^{-1}) for the catalytic oxidation of phenols by the hemin complexes in the presence of hydrogen peroxide (0.1 M phosphate buffer at 25°C)

Complex	1	2	3	L-4*	D-4*
Hemin-A	19 ± 3	26 ± 2	20 ± 3	76 ± 15	80 ± 20
Hemin-B	17 ± 1	80 ± 10	80 ± 10	260 ± 60	250 ± 60
Hemin-C	15 ± 3	38 ± 3	36 ± 4	95 ± 10	100 ± 10
Hemin-D	50 ± 7	45 ± 7	60 ± 15	240 ± 40	230 ± 50

*Data were determined under nonsaturating conditions for limited solubility.

concentration of phenolic substrate, the rate equation for the above catalytic scheme can be reduced to:

$$r = \{(K_p/k'c)k_1'[H_2O_2][E_0]\}/\{((k_p/k_C') + [H_2O_2])\},$$

where $[E_0]$ is the initial concentration of hemin complex. The kinetic parameters that can be obtained by studying the dependence of the substrate oxidation rate on peroxide concentration are the rate constant k_1', measuring the formation rate of the active species in the presence of substrate, and the ratio k_P/k_C', ruling the competition between peroxidase and catalase activity and, therefore, the efficiency of the complex in the peroxidase reaction. The values of these parameters obtained from the kinetic experiments are collected in Tables 2 and 3.

Relaxometric characteristics

A 1.0 mM solution of hemin-C was investigated from the relaxometric viewpoint as a function of pH and temperature. As expected for an $S = 1/2$ system, the millimolar relaxivity r_{1p} at 20 MHz shows a value of 0.30 s^{-1} mM^{-1}, at 25°C and pH 7.0, which is markedly smaller than that reported for hemin-HSA (r_{1p} = 4.8 s^{-1} mM^{-1}) (Fasano et al., 2001). This value is further reduced by increasing the temperature, as expected for a low-spin complex lacking coordinated water molecules. When the pH of the hemin-C solution is increased, a marked change in the solvent water relaxivity is observed (Fig. 2) and a r_{1p} value of 2.28 s^{-1} mM^{-1} is reached at pH ≥ 10. The relaxivity change is consistent with a single equilibrium, with a pK_a value of 8.77 ± 0.07.

Measurements of ^{17}O-NMR linewidth as a function of temperature (data not shown) are consistent with the absence of a coordinated water molecule in the inner sphere of Fe(III) in hemin-C at any pH value. This observation gives further support to the view that a transition from a six-coordinated His_2Fe center to a five-coordinated ferric heme is occurring at basic pH.

Replacement of ferric hemin by its Mn(III) analog allows us to deal with systems endowed with higher relaxivity values. Mn(III)-protoporphyrin complexes are reported to be often in the high-spin state, i.e., with four unpaired electrons (Mashiko and Dolphin, 1987). Therefore, a direct comparison with the full-length Mn(III)-PPIX-HSA derivative can be performed. The millimolar relaxivity of Mn(III)-PPIX-C is almost unchanged at different pH values, except for small fluctuations that could be attributed to conformational transitions in the protein fragment and decrease exponentially with temperature (Fig. 3). The complex Mn(III)-PPIX-HSA (Fasano et al., 2001) displays larger relaxivity values than Mn(III)-PPIX-C at any pH. A possible explanation for both smaller relaxivity and temperature dependence is that Mn(III), like Fe(III), is coordinated by two His residues. To ascertain the lack of any coordinated water molecule, ^{17}O linewidths of Mn(III)-PPIX-C and of diamagnetic fragment C solutions partially enriched in $H_2{}^{17}O$ were measured as a function of temperature. The extent of the paramagnetic contribution to the transverse relaxation of the ^{17}O nucleus is determined by the occurrence of a scalar coupling through the Mn(III)-H_2O coordination bond (Aime et al., 1998, 1999). Because the two solutions show almost identical ^{17}O linewidths, the occurrence of a paramagnetic contribution arising from the exchange of a water molecule directly coordinated to Mn(III)-PPIX has to be discarded. Nevertheless,

TABLE 3 Kinetic constants k_p/k_c' (mM) for the catalytic oxidation of phenols by the hemin complexes in the presence of hydrogen peroxide (0.1 M phosphate buffer at 25°C)

Complex	1	2	3	L-4	D-4
Hemin-A	100 ± 20	28 ± 3	43 ± 2	9 ± 2	9 ± 3
Hemin-B	53 ± 3	16 ± 3	10 ± 2	3 ± 1	4 ± 1
Hemin-C	80 ± 20	20 ± 2	8 ± 1	8 ± 1	7 ± 1
Hemin-D	55 ± 9	21 ± 4	3 ± 1	2.0 ± 0.4	2.0 ± 0.4

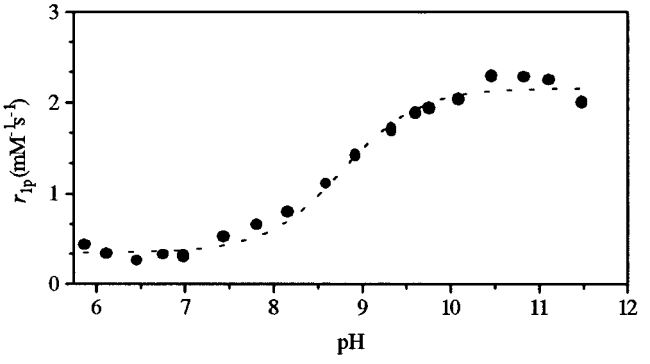

FIGURE 2 Water proton millimolar relaxivity of a hemin-C solution (1.0 mM ferric heme, 1.2 mM fragment C) in PBS at 25°C as a function of pH. The relaxivity increase is consistent with a single equilibrium, and the dotted line indicates a pK = 8.77 ± 0.07 for the change in the spin state of the paramagnetic center.

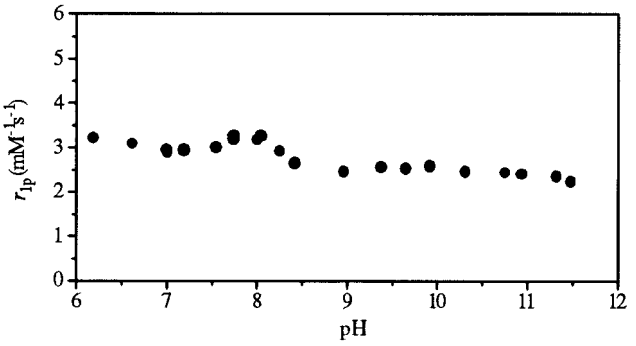

FIGURE 3 Effect of the pH value on the relaxivity for Mn(III)heme-C at 25°C. Fragment C concentration was 1.2 mM in PBS, and Mn(III)-protoporphyrin concentration was 1.0 mM.

we observe a relaxivity value that is even smaller than that observed for Mn(III)-PPIX-HSA at pH 10, i.e., when no directly coordinated water molecules are present. Again, the different contribution of outer sphere water molecules close to the paramagnetic center could be invoked to justify the observed data.

ES/MS analysis of the hemin-C complex

The hemin-C complex, eluted from a PD10 column in 50 mM ammonium acetate, pH 7.0, at a concentration of 10 pmol/μl, was directly analyzed by ion spray mass spectrometry, producing the spectrum shown in Fig. 4. The most abundant species (component *A*) showed a molecular mass of 19,972.1 $\pm$ 1.0 Da, corresponding to the isolated fragment C with Met-298 in its homoserine lactone form. The molecular mass of component *B* was measured as 20,589.2 $\pm$ 1.2 Da, with a mass increase of ~616 Da as compared with fragment C, corresponding to the binding of a single hemin molecule. Moreover, the mass spectrum showed the occurrence of a very minor species (component *C*) whose molecular mass indicated the binding of two hemin molecules to fragment C. The results of this mass spectral investigation indicate that fragment C essentially binds hemin with a 1:1 stoichiometry. The presence of a major species corresponding to the unbound form of fragment C in the spectrum is very likely a result of the partial dissociation of the complex in the gaseous phase during mass spectral analysis. Finally, the occurrence of a minor component with two hemin molecules linked to the protein results from the conditions of excess hemin used in the preparation of the sample. This compound might be interpreted either in terms of the existence of two different hemin binding sites in fragment C or, more likely, by the interaction of a hemin dimer within the same site of the protein, in view of the high tendency of hemin to form dimers in aqueous solution, as demonstrated by ES/MS analysis of dilute hemin solutions (data not shown).

Limited proteolysis and mass spectrometry

The interaction of hemin with fragment C was investigated by a strategy that combines limited proteolysis experiments with mass spectrometric procedures (Zappacosta et al., 1996; Scaloni et al., 1998; Orrù et al., 1999). The overall strategy is based on the evidence that amino acid residues located within exposed and flexible regions of the protein can be recognized by proteases, leading to a good imprinting of the protein conformation in solution. When these experiments are performed on both the isolated protein and a protein complex, one may draw useful insight into conformational changes and/or inaccessibility of protein regions due to binding of the ligand.

Limited proteolysis experiments were performed on fragment C and hemin-C by using trypsin, protease V8, subtilisin, and chymotrypsin as proteolytic probes. The protein

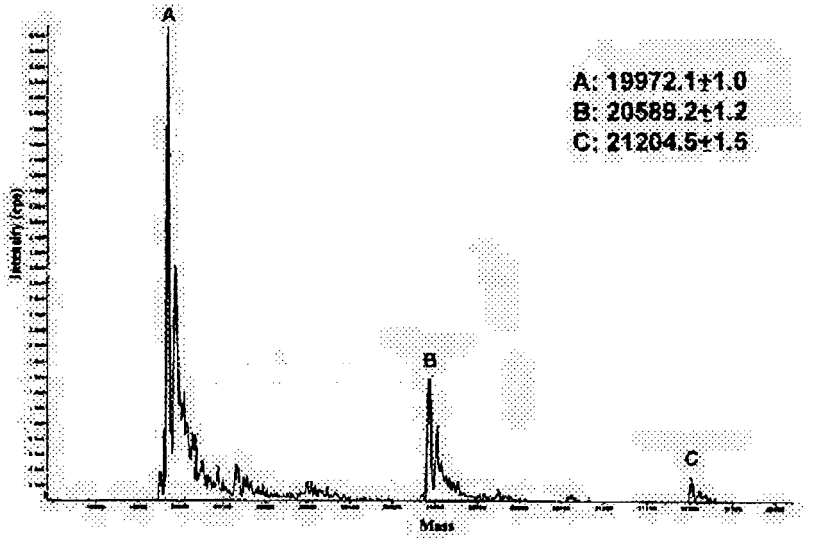

FIGURE 4 Transformed electrospray mass spectrum of the hemin-C complex. The individual species are indicated by capital letters. The molecular masses of the various components are reported.

TABLE 4 Map of the preferential cleavage sites observed in the isolated fragment C and in the hemin-C complex

Protease	Fragment C	Hemin-C
Trypsin	Lys-190, Lys-195, Arg-197	Lys-190, Lys-195, Arg-197
Endoprotease V8	Glu-184, Glu-188, Glu-208,* Glu-227,* Glu-230*	Glu-184, Glu-188, Glu-227,* Glu-230*
Chymotrypsin	Phe-211,* Trp-214,* Leu-219*	Phe-206,* Leu-219*
Subtilisin	Ser-192, Ala-194, Gln-204,* Ser-232*	Ser-192, Ala-194

*Cleavage sites producing excision of internal peptides from the protein owing to the presence of disulfide bridges.

and the complex were incubated with each protease under strictly controlled conditions to ensure the maintenance of native conformation. The extent of enzymatic hydrolysis was monitored by reverse-phase HPLC; the fragments released from the proteins were identified by ES/MS leading to the assignment of the cleavage sites.

Under the controlled conditions used for trypsin hydrolysis of fragment C (E/S 1/1000, w/w) only a few specific fragments were released; ES/MS analysis of individual fractions identified these fragments as peptides 124–190, 124–195, and 124–197. The presence of the complementary peptide pairs 191–298, 196–298, and 198–298, clearly indicates that these fragments originated from single proteolytic events that occurred on the native fragment at the level of Lys-190, Lys-195, and Arg-197. Similar results were obtained with protease V8 as indicated in Table 4. Cleavages at Glu-184 and Glu-188 generated two complementary peptide pairs of fragments whereas the proteolytic events occurring at Glu-208, Glu-227, and Glu-230 caused the excision of internal regions of the protein, because of the presence of the disulfide bridge between Cys-200 and Cys-246.

Additional limited proteolysis experiments were then carried out by incubating fragment C with broader specificity proteases such as chymotrypsin and subtilisin (Table 4). As an example, the mass spectral analysis of the chymotryptic digestion of the protein revealed the occurrence of primary cleavage sites at Phe-211, Trp-214, and Leu-219, as inferred from the identification of the species (124–214)-(220–298) and (124–211)-(215–298), characterized by the presence of a disulfide bridge linking the two peptides.

The experimental approach described above was then used to investigate the surface topology of hemin-C. The complex showed a generally lower accessibility to proteases than the ligand-free HSA fragment, as demonstrated by the higher E/S ratio needed to observe proteolytic cleavages, thus suggesting that the interaction with hemin increased the compactness of fragment C causing a general decrease in the rate of hydrolysis. The preferential cleavage sites observed on the hemin-C complex are listed in Table 4. Compared with fragment C in the apo form, the complex exhibits a similar pattern of cleavage sites within the α-helical region spanning residues from 174 to 205 (h10(I)–h1(II) (Carter and Ho, 1994)), except for Glu-204, which is now inaccessible to proteases, whereas complete protection of the cleavage sites occurs in the region of h2(II), containing Glu-208, Phe-211, and Trp-214.

DISCUSSION

Hemin binds tightly to HSA in a cleft that leaves little space for the addition to the iron center of even small high-affinity ligands (Monzani et al., 2001). The spectral features of the hemin-HSA complex are consistent with an equilibrium between a major high-spin and a minor low-spin species. Reactivity studies using hydrogen peroxide and exogenous substrates confirmed the limited access to the heme (Monzani et al., 2001). The spectroscopic and binding studies carried out on the hemin-D complex, where the protein moiety corresponds to HSA depleted of the C-terminal fragment A, show that this large D fragment, but not the smaller C fragment (Hrkal et al., 1978), contains the entire HSA domain I proposed to act as the hemin binding site (Dockal et al., 1999). Recent studies indicate a contribution from its C-terminal domain IIA, possibly with a histidine and/or a tyrosine acting as iron axial ligands in the major high-spin species (Fasano et al., 2001). The electronic spectral properties and especially the induced CD pattern in the Soret region, which reflects the interactions between the transition moments of the porphyrin and those located in the chromophores of the protein residues in the heme environment, are almost identical for hemin-D (Fig. 1) and hemin-HSA (Casella et al., 1993). The minor differences observed for the two complexes can be ascribed to an increased flexibility in the peptide chain surrounding the heme in fragment D, allowing a somewhat easier approach of the endogenous ligand to the iron center.

This view is supported by the behavior of the hemin-C complex. This protein fragment is smaller than D, as it is further depleted of a consistent portion of the N-terminal polypeptide chain, and contains only part of the hemin binding site located within HSA domain I. Hemin-C appears to be totally low spin, with two imidazole groups acting as protein axial ligands, both of which are probably different from those present in hemin-HSA and hemin-D. The existence of some local mobility in the peptide chain carrying the sixth ligand is shown by the reversible change to a five-coordinated structure observed in basic medium. The lack of formation of a low-spin, hydroxymet species in these conditions, as it is observed, for instance, for the oxygen carrier proteins (Antonini and Brunori, 1971), is highly unusual in heme-protein coordination chemistry and indicates that also for fragment C the protein pocket hosting the heme must be tight and basically inaccessible to small

polar molecules. The opposite CD behavior within the Soret band between the high-spin hemin C derivative in basic medium and the corresponding high-spin components of hemin-D and hemin-HSA complexes is a signature of the different nature of the polypeptide chains around the heme group. A similar trend can be noted also between the induced CD patterns of the low-spin components. The Soret CD band of hemin-C in neutral medium (Fig. 1) is in fact opposite to those of the corresponding low-spin forms of hemin-D and hemin-HSA at the equilibrium in solution.

In addition to the high-affinity binding site, HSA has other heme-binding centers with lower affinity, which can be located in different portions of the polypeptide chain. As shown in the present study, a relatively strong hemin-binding site is present in fragment A and another, less strong, in fragment B. The characteristics of iron coordination in the two cases are different, six-coordinated low spin in hemin-A and five-coordinated high spin in hemin-B, but with histidine residues involved as axial ligands in both cases. However, the lack of any significant CD features for these complexes seem to indicate the existence of more than a single binding site with similar affinity for hemin in these HSA fragments. The reactivity studies performed with hydrogen peroxide and several exogenous substrates confirm that even for hemin-A and hemin-B, as well as for hemin-C and hemin-D, the approach to the heme is basically restricted to molecules of relatively small size such as the phenols investigated here, independently of the absence or presence of charges on their substituents.

Some general comments on the kinetic data are worth mentioning in the present context, because they bear on the structural features of the hemin complexes. The kinetic constant k_1' reflects the differences in the binding site environment of the heme and the activation of acid-base catalysis by the polar substrates. Thus, with *p*-cresol, which lacks polar groups in the substituent, k_1' is very small for all hemin-peptide complexes carrying a low-spin iron center, whereas somewhat larger values are observed for those complexes in which an equilibrium between high-spin and low-spin species exist, i.e., hemin-D (Table 2) and hemin-HSA (Monzani et al., 2001). For substrates 2–4, the k_1' values are generally larger than for 1, indicative of a contribution of acid-base catalysis in the cleavage of the peroxide O-O bond by the polar substituents of the phenol. The k_P/k_C' values are basically controlled by the redox potential of the phenols (Monzani et al., 1997), and in fact the highest activities are observed with the most easily oxidizable substrate 1 (Table 3). In general, it is clear that only the k_1' and k_P/k_C' values exhibited by hemin-D with the various substrates are close to those found for hemin-HSA (Monzani et al., 2001), reflecting a similar arrangement of the substrates near the heme in the catalytic process. For the hemin complexes with the other HSA fragments the differences in the heme environment dictate that also the mode of interaction of the substrates near the heme will be different.

The structural effects determined by cleavage of the N-terminal fragment B of HSA are of some interest because fragment C contains the binding region, termed Sudlow's site I (Sudlow et al., 1975), which is located in domain IIA spanning from residue 199 through 292 of HSA (He and Carter, 1992). Several important ligands are believed to bind in this region; bilirubin, warfarin, and salicylates can be accommodated, and more than one at a time, without significant interference. We therefore decided to investigate in more detail the properties of this hemin-C complex, where the heme group can be exploited as a reporter probe of the protein environment.

The pH-dependent spin state change undergone by hemin-C is expected to dramatically affect the relaxation of solvent water protons in the solution (Fasano et al., 2001; Baroni et al., 2001). The low-spin form present in neutral solution is actually characterized by a very low effect on the relaxation rate of water protons. The millimolar relaxivity r_{1p} at 20 MHz (0.30 s^{-1} mM^{-1}) is significantly smaller than that reported for hemin-HSA (4.8 s^{-1} mM^{-1}) (Fasano et al., 2001), even though a change in the number of mobile hydrogens may contribute to a potential second sphere effect.

With the transition of hemin-C to the high-spin form at basic pH, a marked increase in the solvent water relaxivity is observed (Fig. 2). Actually, the relaxivity value in these conditions (2.28 s^{-1} mM^{-1}) is larger than those reported for most ferric oxygen carriers. In the case of sperm whale (*Physeter catodon*) myoglobin, horse (*Equus caballus*) myoglobin, loggerhead sea turtle (*Caretta caretta*) myoglobin, and human hemoglobin (Aime et al., 1993, 1996), the paramagnetic contribution to the water relaxation rate is in the range of 0.8–1.2 mM^{-1} s^{-1} at 20 MHz. Although the increase of relaxivity with pH is clearly due to a spin-state change, the effect of the $S = 5/2$ paramagnetic center needs to be amplified by some of the residual water molecules that are still buried in the protein core after the cleavage. Therefore, the observed value, which is intermediate between those for ferric, high-spin oxygen carriers and ferric, high-spin hemin-HSA, reflects both a lower reorientational correlation time for the HSA fragment and a smaller number of water molecules contributing to the second sphere effect (Halle et al., 1999).

Replacement of hemin Fe(III) with Mn(III) has a strong influence on the spectral, binding, and relaxometric properties of the protein complexes. Mn(III)-PPIX binds less strongly than hemin to both HSA and fragment D but more strongly than hemin to fragment C. This difference can be attributed to the easier formation of the metal complex with bis-histidine ligation in fragment C. The larger paramagnetism of Mn(III)-PPIX-C produces higher relaxivity effects of water protons compared with its Fe(III) analog, and in addition, for the Mn(III) derivative both the spectral features and relaxivity effects are basically unchanged with pH, indicating that the polypeptide chain carrying the sixth axial ligand is more conformationally rigid than in hemin-C.

Fig. 5 shows a ribbon diagram of HSA fragment C as obtained from the x-ray coordinates of HSA (Protein Data

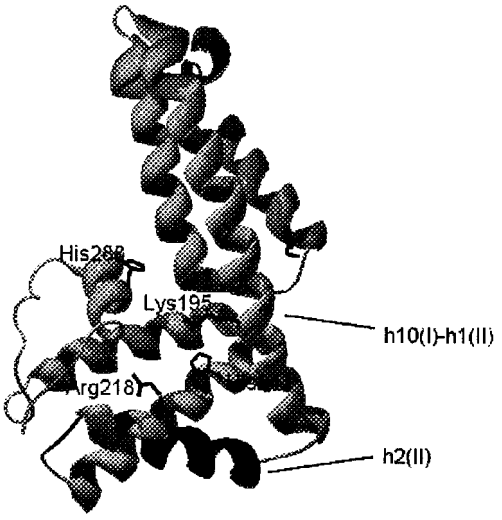

FIGURE 5 Ribbon diagram of the HSA region corresponding to fragment C. Relevant side chains are rendered in sticks. For additional details see text.

Bank code 1bm0) (Sugio et al., 1999). The main feature is the long interdomain helix (namely, h10(I)-h1(II) (Peters, 1996), residues 177–205), which is docked to helices h8(I) and h9(I) to form a three-helix bundle capped by helix h7(I). This motif is orientated perpendicular to the assembly formed by helices h2(II) to h6(II). Obviously, the structural model obtained by simply cutting the atomic coordinates of the fragment from the atomic coordinates of the whole protein is far from being representative of the actual solution structure of fragment C. Moreover, HSA fragments are expected to possess an intrinsic conformational flexibility, because many contacts have been removed.

The results of the spectroscopic, reactivity, and relaxometric studies can thus be combined with proteolysis/MS experiments to forward a suggestion for a potential heme-binding site in the fragment C model. Limited proteolysis data performed on the ligand-free fragment C indicate that preferential proteolytic sites are gathered within helices h10(I)-h1II) and h2(II). A quite similar distribution of cleavage sites was observed within the α-helical h10(I)-h1(II) region for hemin-C, with only Gln-204 being inaccessible in the complex. This finding would suggest that h10(I)-h1(II) is actually solvent exposed in hemin-C. On the contrary, differences were detected in the region of helix h2(II), where Glu-208, Phe-211, and Trp-214 were completely protected from proteases in the complex (Table 4). These data suggest that the region encompassing residues Glu-208 to Trp-214 is involved in the interaction with hemin and, therefore, is protected from the activity of proteases. This helix constitutes a definitely hydrophobic stretch (in black in Fig. 5) and could be indicated as the docking site for hemin to fragment C. If we compare the binding site characteristics of the heme in HSA and fragment D with those in fragment C we note that cyanogen bromide cleavage of the N-terminal HSA portion (B) forces hemin to bind in a protein cleft that is different but just adjacent to that used by HSA and fragment D. This cleft is lined by residues Glu-208, Phe-211, and Trp-214 and constitutes the subpocket in which the benzyl moiety of warfarin is bound, predominantly through hydrophobic contacts (Petitpas et al., 2001). It should be emphasized that the imidazole ring of His-242 (black sticks in Fig. 5) is in close proximity to the hydrophobic pocket defined by these residues and might then constitute the fifth axial ligand to the iron atom. Tyr-148 seems to be accessible to Fe(III), but the different orientation of the porphyrin caused by the new stabilizing contacts makes coordination of this residue unsuitable. A different ligand, with stronger ligand field, occupies the sixth iron coordination position in hemin-C, very likely a second histidine residue. This residue could be His-288 (see Fig. 5), which belongs to a structural element lacking stabilizing contacts with the part of the polypeptide chain that has been removed by the cyanogen bromide cleavage; thus it could rearrange to form the low-spin bis-histidine complex present in this complex. A large flexibility of this region is also suggested by the conformational transition undergone by this complex from neutral to basic pH.

An analysis of the charge distribution indicates that these structural components have opposite charge, with residues belonging to domain I endowed with a positive charge and helices h3(II) to h6(II) with a large negative potential. His-242 is located within the crevice formed by the structural elements with opposite charge distribution, i.e., in a region where the electrostatic potential is lower. Basic residues such as Lys-195 and Arg-218 (see Fig. 5) should contribute to the hemin docking by providing salt bridges to hemin propionates.

In conclusion, the picture emerging from the present comparative studies on HSA fragments indicates that hemin binds to fragment C in the region usually indicated as Sudlow's site I, which is located in proximity to the site where hemin binds to both fragment D and full-length HSA. This is in keeping with the observation that the binding clefts for hemin and warfarin in HSA are functionally and spectroscopically linked (Baroni et al., 2001).

Note that after completion of this work, a structural description of the heme binding site in HSA has been reported at the atomic level (Wardell et al., 2002).

This work was supported by grants of Projetto di Rilevante Interesse Nazionale of the Italian Ministero Università e Ricerca Scientifica e Technologica.

REFERENCES

Aime, S., P. Ascenzi, M. Fasano, and S. Paoletti. 1993. NMR relaxometric studies of heme accessibility to heme cavity in horse heart and sperm whale myoglobin. *Magn. Reson. Chem.* 31:S85–S89.

Aime, S., M. Botta, M. Fasano, and E. Terreno. 1998. Lanthanide (III) chelates for NMR biomedical applications. *Chem. Soc. Rev.* 27:19–29.

Aime, S., M. Botta, M. Fasano, and E. Terreno. 1999. Prototropic and water exchange processes in aqueous solutions of Gd(III) chelates. *Acc. Chem. Res.* 32:941–949.

Aime, S., M. Fasano, S. Paoletti, F. Cutruzzolà, A. Desideri, M. Bolognesi, M. Rizzi, and P. Ascenzi. 1996. Structural determinants of fluoride binding to hemoglobin and myoglobin: crystallographic and proton NMR relaxometric study. *Biophys. J.* 70:482–488.

Antonini, E., and M. Brunori. 1971. Hemoglobin and Myoglobin in Their Reactions with Ligands. North Holland Publishing, Amsterdam.

Balla, J., H. S. Jacob, G. Balla, K. Nath, J. W. Eaton, and G. M. Vercellotti. 1993. Endothelial-cell heme uptake from heme proteins: induction of sensitization and desensitization to oxidant damage. *Proc. Natl. Acad. Sci. U.S.A.* 90:9285–9289.

Baroni, S., M. Mattu, A. Vannini, R. Cipollone, S. Aime, P. Ascenzi, and M. Fasano. 2001. Effect of ibuprofen and warfarin on the allosteric properties of haem-human serum albumin: a spectroscopic study. *Eur. J. Biochem.* 268:6214–6220.

Beaven, G. H., S.-H. Chen, A. D'Albis, and W. B. Gratzer. 1974. A spectroscopic study of the hemin-human serum albumin system. *Eur. J. Biochem.* 41:539–546.

Braun, S., H.-O. Kalinowski, and S. Berger. 1998. 150 and More Basic NMR Experiments. Wiley-VCH, Weinheim, Germany.

Carter, D. C., and J. X. Ho. 1994. Structure of serum albumin. *Adv. Protein Chem.* 45:153–203.

Casella, L., M. Gullotti, S. Poli, and L. De Gioia. 1993. Haem-protein interactions: the binding of haem complexes to serum albumin. *Gazz. Chim. Ital.* 123:149–154.

Casella, L., S. Poli, M. Gullotti, C. Selvaggini, T. Beringhelli, and A. Marchesini. 1994. The chloroperoxidase-catalyzed oxidation of phenols: mechanism, selectivity, and characterization of enzyme-substrate complexes. *Biochemistry.* 33:6377–6386.

Dawson, J. H. 1988. Probing structure-function relations in heme-containing oxygenases and peroxidases. *Science.* 240:433–439.

Dockal, M., D. C. Carter, and F. Rüker. 1999. The three recombinant domains of human serum albumin. *J. Biol. Chem.* 274:29303–29310.

Dockal, M., M. Chang, D. C. Carter, and F. Rüker. 2000. Five recombinant fragments of human serum albumin: tools for the characterization of the warfarin binding site. *Protein Sci.* 9:1455–1465.

Doyen, N., A. J. Pesce, and C. Lapresle. 1982. Immunochemical cross-reactivity between cyanogen bromide fragments of human serum albumin. *J. Biol. Chem.* 257:2770–2774.

Fasano, M., S. Baroni, A. Vannini, P. Ascenzi, and S. Aime. 2001. Relaxometric characterization of human hemalbumin. *J. Biol. Inorg. Chem.* 6:650–658.

Galliano, M., L. Minchiotti, F. Porta, A. Rossi, G. Ferri, J. Madison, S. Watkins, and F. W. Putnam. 1990. Mutations in genetic variants of human serum albumin found in Italy. *Proc. Natl. Acad. Sci. U.S.A.* 87:8721–8725.

Guex, N., and N. C. Peitsch. 1997. SWISS-MODEL and the Swiss-PDB-Viewer: an environment for comparative protein modeling. *Electrophoresis.* 18:2714–2723.

Halle, B., V. P. Denisov, and K. Venu. 1999. Multinuclear relaxation dispersion studies of protein hydration. *In* Biological Magnetic Resonance, Vol. 17. N. R. Krishna and L. J. Berliner, editors. Kluwer Academic/Plenum Publishers, New York.

He, X., and D. C. Carter. 1992. Atomic structure and chemistry of human serum albumin. *Nature.* 358:209–215.

Hrkal, Z., M. Kodicek, Z. Vodrazka, B. Meloun, and L. Moravek. 1978. Haeme binding to human serum albumin and to the three large cyanogen bromide albumin fragments. *Int. J. Biochem.* 9:349–355.

Hrkal, Z., Z. Vodrazka, and I. Kalousek. 1974. Transfer of heme from ferrihemoglobin and ferrihemoglobin isolated chains to hemopexin. *Eur. J. Biochem.* 43:73–78.

Ignarro, L. J., J. N. Degnan, W. H. Baricos, P. J. Kadowitz, and M. S. Wolin. 1982. Activation of purified guanylyl cyclase by nitric oxide requires heme: comparisons of heme-deficient, heme reconstituted and heme containing forms of soluble enzyme from bovine lung. *Biochim. Biophys. Acta.* 718:49–59.

Jacob, H. S. 1994. Newly recognized causes of atherosclerosis: the role of microorganisms and of vascular iron overload. *J. Lab. Clin. Med.* 123: 808–816.

Kadish, K. M., K. Smith, and R. Guilard, editors. 1999. The Porphyrin Handbook. Academic Press, San Diego.

Kuzelova, K., M. Mrhalovà, and Z. Hrkal. 1997. Kinetics of heme interaction with heme-binding proteins: the effect of heme aggregation state. *Biochim. Biophys. Acta.* 1336:497–501.

Lapresle, C., and N. Doyen. 1975. Isolation and properties of a fragment of human serum albumin demonstrating the absence of a methionine residue from some of the albumin molecules. *Biochem. J.* 151:637–643.

Mashiko, T., and D. Dolphin. 1987. Porphyrins, hydroporphyrins, azaporphyrins, phtalocyanines, corroles, corrins and related macrocycles. *In* Comprehensive Coordination Chemistry: The Synthesis, Reaction, Properties and Application of Coordination Compounds, Vol. 2. Pergamon Press, Oxford, UK. 826–828.

Miller, Y. I., and N. Shaklai. 1999. Kinetics of hemin distribution in plasma reveals its role in lipoprotein oxidation. *Biochim. Biophys. Acta.* 1454: 153–164.

Monzani, E., B. Bonafè, A. Fallarini, C. Redaelli, L. Casella, L. Minchiotti, and M. Galliano. 2001. Enzymatic properties of human hemalbumin. *Biochim. Biophys. Acta.* 1547:302–312.

Monzani, E., A. L. Gatti, A. Profumo, L. Casella, and M. Gullotti. 1997. Oxidation of phenolic compounds by lactoperoxidase: evidence for the presence of a low-potential compound II during catalytic turnover. *Biochemistry.* 36:1918–1926.

Ochoa, S., and C. de Haro. 1979. Regulation of protein synthesis in eukaryotes. *Annu. Rev. Biochem.* 48:549–580.

Orrù, S., F. Dal Piaz, A. Casbarra, G. Biasiol, R. De Francesco, C. Steinkühler, and P. Pucci. 1999. Conformational changes in the NS3 protease from hepatitis C virus strain Bk monitored by limited proteolysis and mass spectrometry. *Protein Sci.* 8:1445–1454.

Owens, J. W., and C. J. O'Connor. 1988. Comparison of the electronic and vibrational spectra of complexes of protoporphyrin-IX, hemeoctapeptide, and heme proteins. *Coord. Chem. Rev.* 84:1–45.

Peters, T., Jr.1996. All about Albumin: Biochemistry, Genetics and Medical Applications. Academic Press, Orlando, FL.

Petitpas, I., A. A. Bhattacharya, S. Twine, M. East, and S. Curry. 2001. Crystal structure analysis of warfarin binding to human serum albumin: anatomy of drug site I. *J. Biol. Chem.* 276:22804–22809.

Sassa, S. 1988. Heme stimulation of cellular growth and differentiation. *Semin. Hematol.* 25:312–320.

Scaloni, A., N. Miraglia, S. Orrù, P. Amodeo, A. Motta, G. Marino, and P. Pucci. 1998. Topology of calmodulin-melittin complex. *J. Mol. Biol.* 277:945–958.

Sudlow, G., D. J. Birkett, and D. N. Wade. 1975. The characterization of two specific drug binding sites on human serum albumin. *Mol. Pharmacol.* 11:824–832.

Sugio, S., A. Kashima, S. Mochizuki, M. Noda, and K. Kobayashi. 1999. Crystal structure of human serum albumin at 2.5 Å resolution. *Protein Eng.* 12:439–446.

Wardell, M., Z. Wang, J. X. Ho, J. Robert, F. Rüker, J. Ruble, and D.C. Carter. 2002. The atomic structure of human methemalbumin at 1.9 Å. *Biochem. Biophys. Res. Commun.* 291:813–819.

Zappacosta, F., A. Pessi, E. Bianchi, S. Venturini, M. Sollazzo, A. Tramontano, G. Marino, and P. Pucci. 1996. Probing the tertiary structure of proteins by limited proteolysis and mass spectrometry: the case of minibody. *Protein Sci.* 5:802–813.

Xie, L. Y., and D. Dolphin. 1994. Biological oxidations with heme proteins. *In* Metalloporphyrins Catalyzed Oxidations. F. Montanari, and L. Casella, editors. Kluwer, Dordrecht, The Netherlands. 269–306.